Mixed Ice Accretion on Aircraft Wings

Zaid A. Janjua[1], Barbara Turnbull[1], Stephen Hibberd[2], Kwing-So Choi[1]

[1] *Faculty of Engineering, University of Nottingham, UK.*
[2] *School of Mathematical Sciences, University of Nottingham, UK.*

Abstract

Ice accretion is a problematic natural phenomenon that affects a wide range of engineering applications including power cables, radio masts and wind turbines. Accretion on aircraft wings occurs when supercooled water droplets freeze instantaneously on impact to form rime ice or runback as water along the wing to form glaze ice. Most models to date have ignored the accretion of mixed ice, which is a combination of rime and glaze. A parameter we term the 'freezing fraction', is defined as the fraction of a supercooled droplet that freezes on impact with the top surface of the accretion ice to explore the concept of mixed ice accretion. Additionally we consider different 'packing densities' of rime ice, mimicking the different bulk rime densities observed in nature. Ice accretion is considered in four stages: rime, primary mixed, secondary mixed and glaze ice. Predictions match with existing models and experimental data in the limiting rime and glaze cases. The mixed ice formulation consequently however provides additional insight into the composition of the overall ice structure, which ultimately influences adhesion and ice thickness; and shows that for similar atmospheric parameter ranges, this simple mixed ice description leads to very different accretion rates. A simple one-dimensional energy balance was solved to show how this freezing fraction parameter increases with decrease in atmospheric temperature, with lower freezing fraction promoting glaze ice accretion.

Keywords:
mixed ice, aircraft wings, freezing fraction, glaze, rime

Nomenclature

a	Aerodynamic heating constant
c_a	Specific heat capacity of air
H_{aw}	Air-water heat transfer coefficient
L_f	Latent heat of fusion
c_w	Specific heat capacity of water
x_e	Evaporative coefficient
e_0	Evaporative function derivative
U_∞	Air speed
d	Droplet diameter
T_f	Freezing temperature
k_i	Thermal conductivity of ice
k_w	Thermal conductivity of water
$\dot{M}$	Mass flux of supercooled droplets on the wing
x_s	Sublimation coefficient
r	Rime height

b	Glaze height
h	Water height
w	Limit of unfrozen water droplets for secondary mixed ice
t_w	Rime transition time
t_b	Primary mixed transition time
α	Angle of attack
β	Collection efficiency
ρ_l	Liquid water content
ρ_w	Density of water
ρ_i	Density of glaze ice
ρ_r	Density of rime ice

1. Introduction

Ice accretion is a natural phenomenon that affects a wide range of external engineering structures, such as aircraft, power cables, radio masts and wind turbines. A motivation for the modelling described in this paper, is to develop an understanding of the basic physical processes leading to ice accretion to inform strategies for improving anti-icing techniques.

The ice accretion process is not straightforward with different types of ice growing under different environmental conditions. Rime ice results from a relatively simple heat transfer process, whereby supercooled water droplets freeze instantaneously on impact with any very cold wing surface [1, 2, 3, 4, 5]. This process creates a relatively low density, porous ice with a distinctive white appearance. In contrast, glaze ice typically grows at temperatures closer to the melting point via a Stefan-type boundary condition, to form a dense and translucent ice layer. Glaze formation requires the presence of water, either due to partial freezing of the supercooled water droplets, or as *runback* water as the electrothermal systems in the leading edge melt any ice structures accreted there. In practice, the ice that forms on an aircraft wing tends to be a combination of rime and glaze ice; potentially with some retained pockets of air and described as *mixed ice.* The inclusion of porosity of rime ice is similar to the approach of Rios (1991) [6] who developed a density formula for accreted ice but did not define different stages of ice accretion. Commercial icing codes such as LEWICE, TRAJICE, ONERA and ICECREMO code [7, 8, 9, 10, 11] have been developed over a number of years. The first three icing codes employ a Messinger [1] approach which includes limitations such as non inclusion of the conduction term in the energy balance, freezing fraction is assumed constant through out accretion and inaccurate description of water movement [12]. The ICECREMO code considers the dynamic behaviour of the runback water film on the accretion rate and uses a Stefan [13] condition at the ice-water interface to overcome these limitations. Thus this will form a basis for our analysis. The ICECREMO code modelled solidification of the runback water film, which resulted in a wider applicability of the model to different icing conditions. However, all of these models however tend to over-predict ice accretion, leading to potential energy wastage through over-use of the electro-thermal de-icing system. A limitation is these do not differentiate between different ice types - an important consideration when considering adhesion to possible wing coatings. More recently, Zhang et al. (2017) [14] included the effects of runback water and porosity of rime ice in the accretion process.

This paper considers the formation of mixed ice on an aircraft wing from the partial freezing of impinging supercooled droplets, which deposit onto the growing interface as a combination of solid rime ice particles and water. We characterise this as a multiphase layer comprising a porous medium created by the solid rime ice particles and water at longer accretion times and different atmospheric conditions. This is in contrast to more traditional ′spongy ice′ models that envisage unfrozen water from supercooled droplets entrapped within the growing ice dendrites [15]. We note mushy layers as seen in sea ice for example, form due to a secondary diffusive process at the solidification front with a presence of multiphase microstructures [16]. Although not explicitly modelled, a multiphase porous medium can provide additional insight towards the inclusion of a mushy structure in future icing models. Generally the water within a rime ice matrix can solidify as glaze ice within the pore space. A solidifying glaze ice grows through the rime particles to create a layer of co-existing rime and glaze, i.e. mixed ice. Anderson and Feo (2002) [17] also included varied freezing fraction values to determine water film thickness and ice shape without defining different stages of ice accretion. In this work we determine a model for the growth rate and accretion based on prevailing atmospheric conditions. Including the

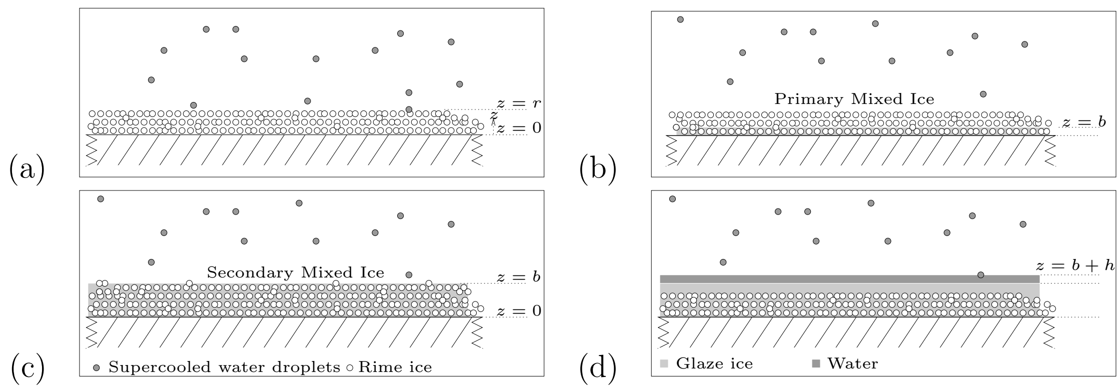

Figure 1: Schematic representation of the modes of accretion in mixed ice formation. (a) At times $t < t_w$, supercooled droplets freeze on impact with the wing, forming rime ice (with air in the pore space). (b) When the layer of rime ice is thick enough that the latent heat released on freezing can no longer be conducted through it, a proportion of the incoming supercooled droplets remain as water. This water quickly freezes as glaze ice within the pore spaces of the original rime layer ($t_w \geq t < t_b$). (c) Once the glaze ice fully occupies the pore space between the rime crystals, rime and glaze can accrete simultaneously in a mixed ice layer, with better thermal conductivity than the rime ice alone. (d) Once this *mixed ice* layer is again too thick to transport released latent heat on the droplets freezing, a water film forms on its surface. This may be supplemented by runback water formed by melting ice formations at the wing leading edge.

formation of a porous ice matrix layer within this model enables more general possibilities to explore in the future, such as forced convective transfer modes.

2. Model Formulation

In this section we introduce four, possibly consecutive, modes of ice accretion within the context of an application to icing on aircraft wings; including any aircraft passing through cloud cover, where the local temperatures can be very cold and available water droplets are supercooled. As the aircraft progresses, these water droplets may impinge on the wing surface. For simplicity, we restrict our initial interest to one-dimensional accretion with calculation of the time evolution of ice growth normal to the wing surface; assuming that the ambient conditions and influx of droplets are steady. A first aim is to understand the influence of rime versus glaze versus mixed accretion modes on the resulting accretion profiles.

2.1. Rime Ice

In the earliest stage of accretion, the wing is approximately at the temperature of the ambient air and the supercooled droplets collected will freeze on impact to form rime ice [7], as illustrated in Fig. 1(a). The wing is generally an effective thermal conductor, so the latent heat released as the supercooled droplets solidify is easily transported away.

A key feature of rime r is that air is generally trapped within the pore spaces between tiny crystals of ice. Thus we define a solid volume fraction of ice in this rime layer

$$\phi = \frac{\rho_r}{\rho_i}, \tag{1}$$

where ρ_r is the bulk density of the rime ice layer and ρ_i is the density of pure ice (we assume that all ice, rime particles or glaze, has density ρ_i, which is independent of temperature). For typical values of opaque rime bulk density, $\rho_r \geq 610\,\mathrm{kg\,m^{-3}}$ [18], the equivalent solid volume fraction follows, $\phi \geq 0.67$. This is consistent with the maximum packing fraction of spheres [19].

For simplicity, we consider one-dimensional accretion on a flat plate, varying with time. The rate of growth of the rime front at $z = r$ (Fig. 1(a)) is given by a mass balance

$$\frac{\partial r}{\partial t} = \frac{1}{\rho_i \phi} \dot{M}, \tag{2}$$

where $\dot{M}$ is the mass flux of incident water droplets. For constant values of $\dot{M}$ and ϕ, the ice height thickness follows,

$$r = \frac{\dot{M} t}{\rho_i \phi}. \tag{3}$$

where t is the elapsed time and $r(t = 0) = 0$.

2.2. Mixed Ice

Rime ice will continue to accrete as in Sec. 2.1 (Fig. 1(a)) until the layer becomes sufficiently thick that the latent heat released on solidification of the droplets can no longer be conducted away through the wing; the top surface of the rime is now at the freezing temperature T_f [20]. This transition time, t_w, can be evaluated from an energy balance (Sec. 2.3).

At the surface interface, only a proportion λ of the incoming supercooled droplets freeze. Subsequently water forms alongside the rime ice and the ice becomes '*mixed*'. This water can percolate through the pore space in the rime layer and freeze as glaze ice inside the pore space (Fig. 1(b)). For simplicity, we assume that there is no air in the ice accretion, but in our model it would be straightforward to include air (as an essentially free parameter). This may be important since observations indicate air occupying up to 35% of the total interstitial space for rime accretion [21]. Such a glaze freezing process inside the pore space occurs over a short timescale and is not explicitly modelled.

Once the glaze ice front reaches the top of the rime (Fig. 1(c)) mixed ice will continue to grow. Rime and glaze form alongside each other in the form of secondary mixed ice because the conduction through the glaze ice freezes all of the unfrozen water at the air-rime interface initially. As the rate of conduction reduces with the increase in ice thickness; eventually, a water film begins to appear within the interstitial rime matrix, above the growing glaze. This can rapidly lead to the film occupying the porous spaces and flowing above the rime matrix as well when the packing fraction is high and freezing fraction is low.

At longer accretion times (Fig. 1(d)), a water film may grow above the rime boundary. Subsequent supercooled droplets will impact on a water film directly instead of the rime matrix and both rime and glaze will accrete simultaneously.

Thus, the freezing fraction λ provides a dimensionless quantity for the fraction of a supercooled droplet that solidifies on impact with the aircraft wing or ice layer. λ depends on the energetics of droplet impact. This is different to the freezing fraction as the ratio of the amount of ice formed to the mass flux of incoming supercooled droplets, describing the solidification process of glaze ice [10]. λ in contrast determines both the rate and type of ice formation which will be apparent in our subsequent discussion.

2.3. Energy Balance

While the water and ice (both glaze and rime) layers remain thin, we can assume that conduction across the layer is the primary mode of heat transfer. The reduced pseudo-steady state conduction equations for heat transfer through the ice and water layers are

$$\frac{\partial^2 T}{\partial z^2} = 0, \tag{4}$$

and

$$\frac{\partial^2 \theta}{\partial z^2} = 0, \tag{5}$$

where T and θ are the temperatures in the ice and water layers respectively [10]. Considering first the early stage of rime accretion (Fig. 1(a)), the temperature distribution through the rime layer is determined by fixing the rime temperature at the wing to be the wing surface temperature (i.e. the ambient air temperature), $T(z = 0) = T_a$. Further, the heat flux through the air-rime interface is determined by an energy balance there [10, 20],

$$\left.\frac{\partial T}{\partial z}\right|_{z=r} = \frac{1}{k_i}\left[Q_l + Q_k + Q_a - (Q_r + Q_h + Q_s)\right], \tag{6}$$

where

Q_k	$= \frac{1}{2}\dot{M}U_\infty^2$	is the droplet kinetic energy,
Q_a	$= \frac{1}{2c_a}aH_{aw}U_\infty^2$	is the aerodynamic heating,
Q_l	$= \lambda\dot{M}L_f$	is the release of latent heat,
Q_d	$= c_w(1-\lambda)\dot{M}(T-T_d)$ $= q_d(1-\lambda)(T-T_a)$	is the droplet thermal energy after stage one of rime accretion ($q_d = c_w\dot{M}$),
Q_r	$= c_w\lambda\dot{M}(T-T_d)$ $= q_r\lambda(T-T_a)$	is the droplet thermal energy during stage one of rime accretion ($q_r = c_w\dot{M}$),
Q_h	$= H_{aw}(T-T_a)$ $= q_h(T-T_a)$	is the convective heat transfer from rime to air,
Q_s	$= x_s e_0(T-T_a)$ $= q_s(T-T_a)$	is the heat of sublimation ($q_s = x_s e_0$),
Q_i	$= c_w\lambda\dot{M}(T_f-T_d)$ $= \lambda q_d(T_f-T_a)$	is the energy to raise the temperature of solidifying fraction of the droplet to the freezing point after stage one of rime accretion.

For pure rime accretion $\lambda = 1$ in the above. Myers (2001) [10] and Myers & Charpin (2004) [20] show that Eqn. 6 can be simplified in the form

$$\frac{\partial T}{\partial z} = E_{rz} - F_{rz}T, \tag{7}$$

where

$$E_{rz} = \frac{1}{k_i}\left[Q_k + Q_a + Q_l + q_r T_d + (q_h + q_s)T_a\right], \tag{8}$$

and

$$F_{rz} = \frac{1}{k_i}\left(q_r + q_h + q_s\right). \tag{9}$$

Solving the conduction equation (Eqn. 4) for T subject to the fixed temperature at the wing surface and flux determined by the simplified energy balance (Eqn. 7),

$$T = T_a + \frac{E_{rz} - F_{rz}T_a}{1 + F_{rz}r} z, \tag{10}$$

within the pure rime layer at $0 \leq z \leq r$.

After a period of rime accretion, water will first appear when the air-rime interface reaches the freezing temperature, i.e. $T(z = r_w) = T_f$ [20]. Thus

$$r_w = k_i \frac{T_f - T_a}{Q_l - Q_r + Q_a + Q_k - (q_h + q_s)(T_f + T_s)}, \tag{11}$$

with a corresponding transition time from the rime mass balance (Eqn. 3)

$$t_w = \frac{\phi \rho_i r_w}{\dot{M}}. \tag{12}$$

At times $t > t_w$, some of the supercooled water droplets must remain as water and $0 \leq \lambda < 1$. This is now the regime for the mixed ice accretion. However, under a range of ambient conditions, water could form within the rime layer before this transition time. The atmospheric conditions required for complete, partial or no freezing of the supercooled droplets, and the resulting ice type that forms is described in Sec. 2.4 and summarised in Table 1.

Assuming that glaze ice freezes quickly within the pore space of deposited rime ice, the propagation of the glaze ice through the rime is determined by a mass balance (Fig. 1(b)). Under steady conditions, glaze ice (b_b) will thus reach the top surface of the accretion at a time

$$t_b = t_w + \frac{(1-\phi)\,\rho_i b_b}{(1-\lambda)\,\dot{M}}, \tag{13}$$

where at this time

$$r_b = r_w + \frac{\lambda \dot{M}\,(t_b - t_w)}{\rho_i \phi}. \tag{14}$$

To complete the specification to determine r_b, b_b and λ, we modify the surface conditions of the energy balance (Eqns. 8 and 9) by including terms Q_i and $q_d T_d$ so as to account for the energy of partially frozen droplets at the air-ice interface,

$$E_{rm} = \frac{1}{k_i}\left[Q_k + Q_a + Q_l - Q_i + q_d T_d + (q_h + q_s) T_a\right], \tag{15}$$

and

$$F_{rm} = \frac{1}{k_i}[q_d + q_h + q_s]. \tag{16}$$

A modification of Eqn. 7 gives the flux condition

$$\frac{\partial T}{\partial z} = E_{rm} - F_{rm}T. \tag{17}$$

Solving Eqn. 4 with the flux condition as in Eqn. 17 and a fixed temperature at the wing surface gives

$$T = T_a + \frac{E_{rm} - F_{rm}T_a}{1 + F_{rm}r} z \tag{18}$$

Substituting for $T = T_f$ at $z = r$, the explicit formula for λ during Stage 2 of accretion is given by rearranging Eqn. 18

$$\lambda = \frac{1}{Q_l}\left\{ \left[\frac{1}{r} + \frac{1}{k}(q_d + q_h + q_s)\right]\left[k_i(T_f - T_a)\right] - Q_a - Q_k \right\}, \tag{19}$$

Eqn. 19 together with the mass balance Eqn. 13 and 14 allows us to solve for λ, r_b and b_b during the second stage of accretion.

Any water layer formed over the ice surface after the secondary mixed ice accretion stage, will interact with the air flow over the wing. The water film does not affect the wing surface boundary condition, which remains $T_s = T_a$, as for the rime accretion case. At the growing ice front $z = b$, the temperature in both the ice and water phases is the freezing temperature, $T(z = b) = \theta(z = b) = T_f$. Integrating Eqn. 4 subject to these boundary conditions, the temperature in the ice layer becomes

$$T = \left(\frac{T_f - T_s}{b} \right) z + T_s, \tag{20}$$

for $0 \leq z \leq b$.

The water film on top of this glaze ice is at the freezing temperature at the ice front and T at its upper surface, $z = b+w$, the heat flux is determined by an energy balance

$$\left. \frac{\partial \theta}{\partial z} \right|_{z=b+h} = \frac{1}{k_w} \left[Q_l + Q_k + Q_a - (Q_i + Q_d + Q_h + Q_e) \right], \tag{21}$$

where $Q_e = x_e e_0 (\theta - T_a) = q_e (\theta - T_a)$ is the heat of evaporation. The difference between this heat flux boundary condition and that for the rime growth at $z = r$, is that evaporation replaces sublimation due to the water film replacing ice at the exposed surface. Eqn. 21 can be simplified to give

$$\frac{\partial \theta}{\partial z} = E_{gz} - F_{gz} \theta, \tag{22}$$

where

$$E_{gz} = \frac{1}{k_w} \left[Q_k + Q_a + Q_l - Q_i + q_d T_d + (q_h + q_s) T_a \right], \tag{23}$$

and

$$F_{gz} = \frac{1}{k_w} \left(q_d + q_h + q_e \right). \tag{24}$$

Taking conduction is the leading heat transfer mechanism (Eqn. 5), the boundary conditions determine the temperature in the water layer as

$$\theta = T_f + \frac{E_{gz} - F_{gz}T_f}{1 + F_{gz}h}\left(z - b\right), \tag{25}$$

for $b \leq z \leq b + w$.

2.4. Freezing Fraction

Ultimately, the freezing fraction λ determines the type of ice accretion in this model, but its value is determined by the prevailing conditions. For example, the water temperature Eqn. 25, is physically constrained. If theoretically a water film exists above the freezing temperature, then both $h > 0$ and $\theta \geq T_f$, implying that $F_{gz}T_f \leq E_{gz}$. From their definitions, Eqn. 25 can be re-written

$$T_f - T_a \leq \frac{Q_k + Q_a + Q_l}{q_d + q_h + q_e}. \tag{26}$$

Since Q_l and q_d are dependent on λ, we thus have ambient constraint on the value λ can take given typical ambient conditions for icing on an aircraft wing [20]. Pure rime forms at very cold temperatures, until a water layer would be thermodynamically possible, as dictated by this inequality. Thus $\lambda = 1$ is possible if $T_a \leq -15.3$°C. At temperatures greater than this, some glaze ice will be present and the overall accretion will be mixed in appearance. Conversely, pure glaze ice corresponding to $\lambda = 0$ will form if $-1.8 \leq T_a \leq 0.0$°C. -1.8°C is thus the highest ambient temperature at which mixed ice can form. These constraints are summarised in Table 1.

Myers & Charpin (2004) [20], Myers (2001) [10] and Myers & Hammond (1999) [9] evaluate from their respective models the highest ambient temperature for pure rime accretion as $-16.6°$C, $-18.35°$C and $-15.98°$C, fitting with our analysis. Data from observations of actual inflight icing also supports our predictions. For example, Lynch & Khodadoust (2001) [22] reported pure glaze accretion in the temperature range $-3 < T < 0°$C where Mirzaei et al (2009) [23] suggest temperatures close to $0°$C.

Now that we know the approximate ranges for mixed ice accretion, we can analyse the composition of mixed ice at ambient temperatures in the range $-15.3 < T_a < -1.8°$C, if and when it grows above r_w, the originally deposited rime layer. If we assume the water film is isothermal at T_f and exists only when $t > t_w$, such that water is well mixed and thereby isothermal [10], the proportion of the incoming droplets that will freeze

$$\lambda_m = \frac{(T_f - T_a)(q_d + q_h + q_e) - Q_k - Q_a}{Q_l}. \tag{27}$$

Thus, for the typical environmental conditions in Table A, we can thus predict that mixed ice accreting at $-5, -10$ and $-15°$C has $\lambda_m = 0.24, 0.61$ and 0.98 respectively.

The physical implications of this are open to debate, but adhesion tests indicate that rime ice and mixed ice or glaze ice have very different properties and would require different approaches to anti- or de-icing. The nature of the bond between the ice and the wing surface, in particular the proportion

Table 1: Ice type variation with droplet freezing fraction, λ.

Droplet Freezing Fraction	Type of Ice	Ambient Temperature Range, °C
$\lambda = 1$	Ice Crystals	$T_a \leq -40.0$
$\lambda = 1$	Rime	$-40.0 \leq T_a \leq -15.3$
$0 \leq \lambda \leq 1$	Mixed	$-15.3 \leq T_a \leq -1.8$
$\lambda = 0$	Glaze	$-1.8 \leq T_a \leq 0.0$
$\lambda = 0$	No Freezing	$0.0 \leq T_a$

of glaze ice present to increase the strength of that bond, could be a significant consideration in optimising strategies. In reality, icing encounters below -20°C are extremely rare [24], the temperature range we consider applying to the overwhelming majority of commercial aircraft applications falls within this mixed accretion band.

2.5. Secondary Mixed Ice

It is useful to differentiate the early-deposited mixed ice that grows through the rime layer with a '*secondary*' mixed ice that accretes after t_b due to partially freezing supercooled droplets. This consists of the simultaneous deposition of a matrix of rime ice, with water freezing in its pore space as glaze ice.

At times $t > t_b$, the growth rate of the rime matrix follows the rime accretion rate of primary mixed described in Eqn. 14, with $\lambda = \lambda_m$ as discussed in Sec. 2.4, i.e.

$$r = \frac{\lambda_m \dot{M} \left(t - t_b\right)}{\rho_i \phi} + r_b. \tag{28}$$

The next stage is to determine the level of the unfrozen portion of the supercooled droplets that impact the air-rime interface before incorporating conduction via the Stefan condition [20]. The condition implies that the velocity of the boundary of phase change is proportional to the temperature gradients across it. This is because either the unfrozen portion will occupy a space within the rime matrix or will fill this space up and engulf the rime matrix. The limit of the unfrozen supercooled droplets is given by w,

$$w = \frac{(1-\lambda_m)\dot{M}\,(t-t_b)}{\rho_w(1-\phi)} + r_b. \tag{29}$$

If $w \geq r$, we define the new limit as $u = r + h_w$ where h_w is given by,

$$h_w = (1-\phi)(w-r). \tag{30}$$

The glaze ice growth rate is determined by a Stefan condition [25] matching the rate of release of latent heat as the liquid solidifies to the rate at which that heat can be transported from the glaze solidification front. After fixing the limit of w, we incorporate a single time step of glaze ice growth b due to Stefan conduction. While w is within r, b is given by

$$(1-\phi)\rho_i L_f \frac{\partial b}{\partial t} = k_i \frac{\partial T}{\partial z}, \tag{31}$$

which can be integrated with conditions $b = r_b$ at $t = t_b$ to give the location of this ‘glaze front’ here b_m as thus.

$$b_m = r_b + \sqrt{\frac{2k_i(T_f - T_s)(t - t_b)}{(1-\phi)\rho_i L_f}}. \tag{32}$$

and if w is outside r, b is given by

$$\rho_i L_f \frac{\partial b}{\partial t} = k_i \frac{\partial T}{\partial z}, \tag{33}$$

where the term on the right hand side corresponds to the transport of heat through the already-formed ice behind the front. Conduction through the water film is neglected since it is typically small, and since the water film is approximately isothermal, [10],

$$b_m = r_b + \sqrt{\frac{2k_i(T_f - T_s)(t - t_b)}{\rho_i L_f}}. \tag{34}$$

A water film appears when the limit of b_m is less than w. This implies that there is now some unfrozen water within the rime matrix or overlying; ice will grow underneath and the amount of heat conducted away through the ice to the wing is insufficient to freeze all of the unfrozen supercooled droplet fraction. When w is less than b_m, we do not differentiate between the rime and glaze fronts since the process is so rapid that everything freezes almost instantaneously. The mass balance for glaze ice accretion (Stage 4 of ice accretion) when the glaze ice and water remain within the rime matrix can be given by

$$\dot{M} = (1-\phi)\rho_i \frac{\partial b}{\partial t} + (1-\phi)\rho_w \frac{\partial w}{\partial t} + \phi \rho_i \frac{\partial r}{\partial t}. \tag{35}$$

2.6. Accretion Types

The atmospheric conditions given in Table 1 show three possible accretion regimes. At cold atmospheric temperatures, $T_a \leq -15.3°$C, only rime ice can form. Thus, accretion follows Eqn. 3 under steady conditions.

Conversely, if the atmospheric temperature is close to the freezing point, $-1.8 \leq T_a \leq 0°$C, incoming droplets deposit as water which then forms glaze ice. The mass balance described in Eqn. 35, where the solid volume fraction $\phi \approx 0$, describes the total ice and water layer with the Stefan solidification condition, Eqn. 35, determining the extent of the glaze ice within this. This model is the one employed in most current major icing codes, such as glaze ice model [10] and includes conduction through the water film unlike our model.

In intermediate conditions, $-15.3 \leq T_a \leq -1.8°$C, mixed ice forms, described by the model we have introduced here. Thus initially, for $t \leq t_w$, rime ice forms following Eqn. 3 until $r = r_w$. At this point, λ decreases as glaze ice forms in the previously deposited rime pore space, until $t = t_b$ and the (primary) mixed ice thickness $b = b_b = r_b$ (Eqns. 13 and 14). Now, glaze and rime continue to grow simultaneously as secondary mixed ice, with freezing fraction λ_m. Rime and glaze ice heights are described by Eqns. 28 & 35 & 34 respectively where applicable.

3. Results and Analysis

In the following, we describe the variation in accretion profile of mixed ice with variation in ambient conditions. We describe A) the initial rime accretion phase at $0 \leq t \leq t_w$, B) a primary mixed accretion phase at $t_w \leq t \leq t_b$, C) a secondary mixed accretion phase at $t_b \leq t \leq t_m$ and finally (D), a glaze accretion process when $t \geq t_m$.

Figure 2(a) shows the ice accretion profile at an ambient temperature of -5°C and rime packing fraction $\phi = 0.65$. The accretion time of 100 seconds shows a clear transition between the various stages such as the rime stage (0–13 s), primary mixed stage (13–35 s), secondary mixed stage (35–68 s) and glaze stage (68–100 s). Figure 2(b) shows accretion for the same conditions as Figure 2(a) but assumes air bubbles of $\phi_a = 0.3$ in Stage B respectively. We can see the inclusion of air in ice freezing from the substrate upwards results in the reduction of primary mixed ice stage time from 22 s to 7 s for $\phi_a = 0.3$. Figure 3(a) shows how the freezing fraction λ changes with time for the conditions in Figure 2(a). After the initial rime stage, λ steadily decreases during primary mixed stage as the ability to conduct latent heat away from the air-rime interface through the rime decreases. The decrease will be more dramatic with higher values of ϕ since the porous space will be filled up quicker by the unfrozen supercooled droplets.

For the secondary mixed and glaze stages, our model assumptions lead to a constant value of λ which is dependent only on the atmospheric temperature since the air-ice or air-water interface is fixed at the freezing temperature

T_f. Figure 3(b) describes the temperature profile during the different stages of accretion for conditions described in Figure 2(a). We can observe that the transition from rime to primary mixed occurs when the temperature of the air-rime interface reaches T_f, according to Myers (2001) [10]. The temperature profile through the glaze growing from the wing upwards during primary mixed follows a linear profile dependent on the location of the top interface. A linear temperature profile is also apparent during the secondary mixed and glaze stages with water film assumed isothermal at T_f.

It has been reported that just 0.13 mm and 0.77 mm of ice accretion can reduce lift characteristics of an aircraft in flight by 20% and 40% respectively [26]. Several devices currently exist to detect ice near the leading of the wing to aid in the visual capacity of crew members including cylinders, sensors using stiffness, hot rods etc. Modern optical sensors provide a consistent signal at 1.27 mm of ice thickness [27]; while ultrasonic sensors under development in a high frequency mode of 2 MHz are sensitive to even 0.2 mm of ice accretion [28]. It is for this reason that the key comparative portion of this analysis focuses on what we term as the 'rapid accretion' phase of 30 seconds when the aircraft is descending or ascending through a cloud structure containing supercooled droplets. After this time period, the aerodynamic characteristics are negatively affected and the ice detection and protection systems begin functioning to mitigate the problem.

Figure 4(a) and figure 4(b) show ice growth under different conditions of ambient temperature and packing fraction with accretion time of 30 seconds.

Figure 5(a) and Figure 5(b) provide a comparison between the ice growth in the author's model and the traditional glaze ice model [10] with $\phi = 0.96$ and ambient temperature of -3°C and -6°C respectively.

We can determine the influence of the two key parameters: packing fraction and ambient temperature on the ice accretion rate and time and transition between different ice regimes. When comparing Figure 4(a) and Figure 5(a), we can see that an increase in the packing fraction from 0.65 to 0.96 while the temperature is fixed at -3°C causes no reduction in overall ice height. The former however sees a prolonged primary mixed stage owing to the lower value of ϕ as compared to the latter. Similarly, comparing Figure 4(b) and Figure 5(b),we can see that an increase in the packing fraction from 0.65 to 0.96 while the temperature is fixed at -6°C causes a reduction in rime and glaze ice height by 21% and 33% respectively. For both cases, it is apparent that higher values of ϕ result in longer rime ice stage, smaller primary mixed stage and drastically affects the ice height; thereby affecting the adhesion characteristics of the accreted ice immensely.

When comparing Figure 4(a) and Figure 4(b), we find that the decrease in temperature from -3°C to -6°C, whilst the packing fraction is kept constant at 0.65, results in an overall ice height of 1.4 mm (1 mm glaze and 0.4 mm mixed) and 1.9 mm (0.6 mm glaze and 1.3 mm rime) respectively. There is a change in the accretion height of glaze and the former case also makes an earlier transition to secondary mixed which is understandable as this is a pre-requisite to moving onto a glaze ice stage which is favoured at higher

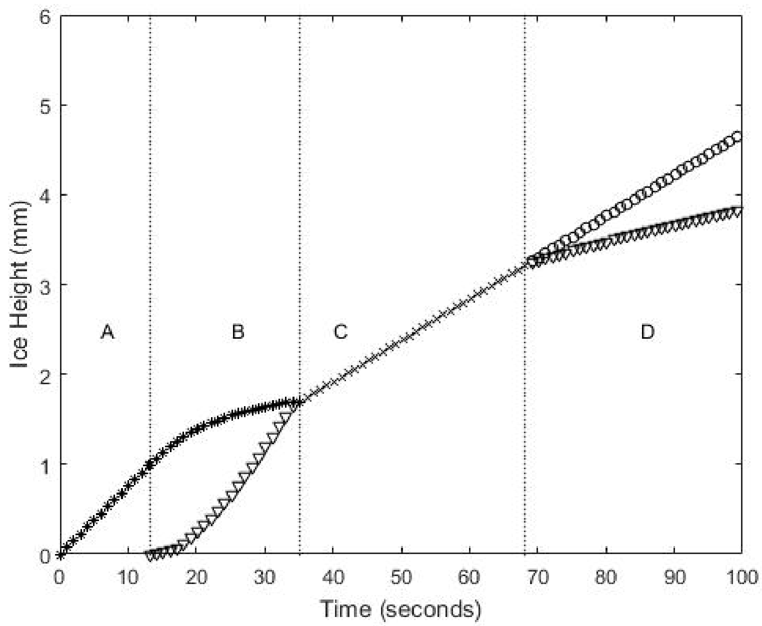

(a)

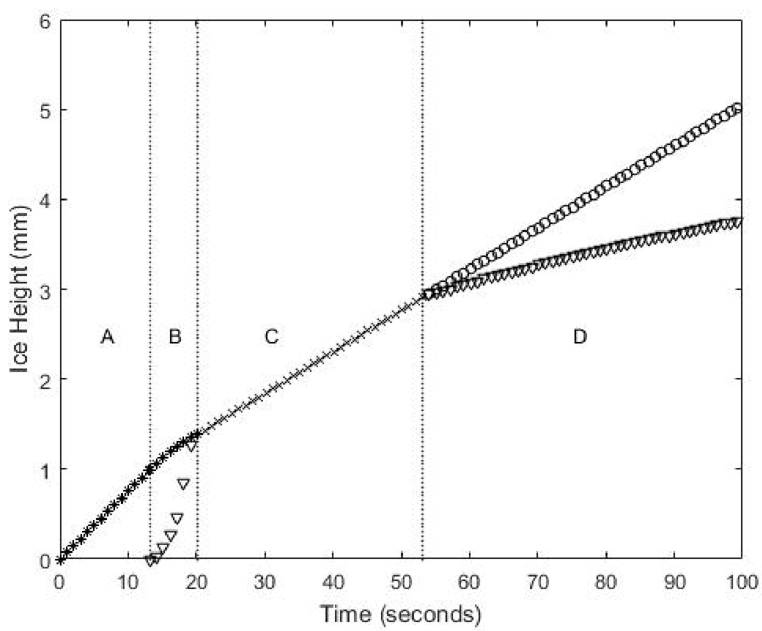

(b)

Figure 2: Mixed ice accretion at T_a = -5°C and $\phi = 0.65$ for 100 s of droplet impingement. The different ice and water limits are represented by the following symbols: rime ($*$), glaze ($\bigtriangledown$), mixed (x) and water film ($\circ$). (a) The ice profile in four different stages. (b) The ice profile with air bubbles occupying $\phi = 0.3$ in Stage B.

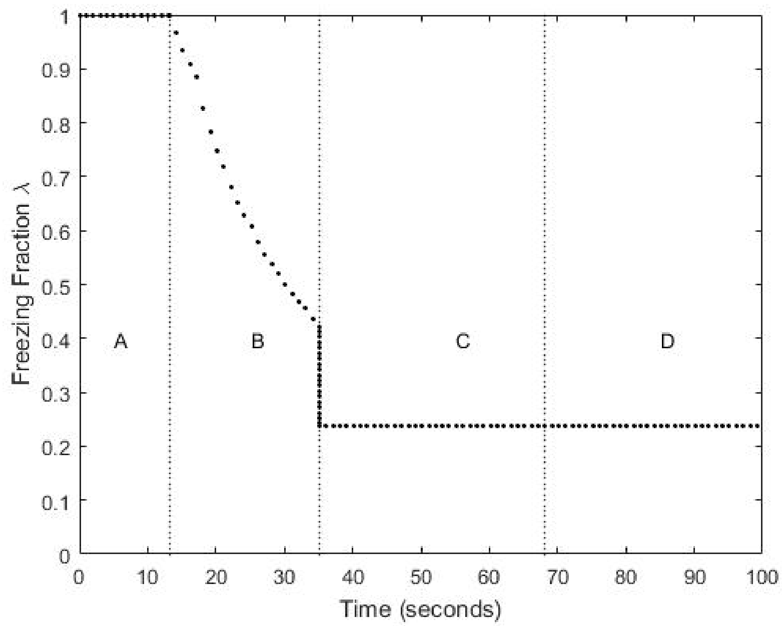

(a)

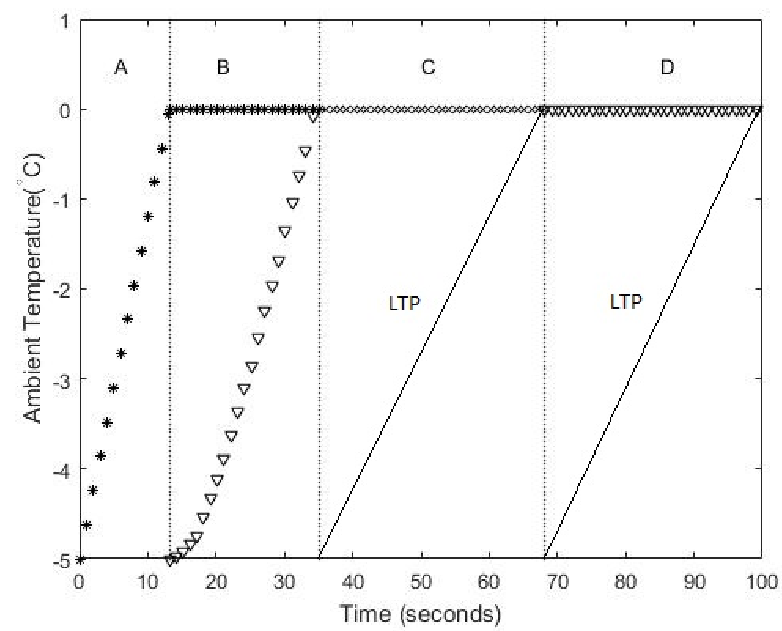

(b)

Figure 3: Mixed ice accretion at T_a = -5°C and $\phi = 0.65$ for 100 s of droplet impingement. The different ice and water limits are represented by the following symbols: rime ($*$), glaze ($\bigtriangledown$), mixed (x) and water film ($\circ$) in (b). (a) The freezing fraction for Figure 2(a). (b) Temperature profile through ice for Figure 2(a). LTP stands for linear temperature profile through the ice.

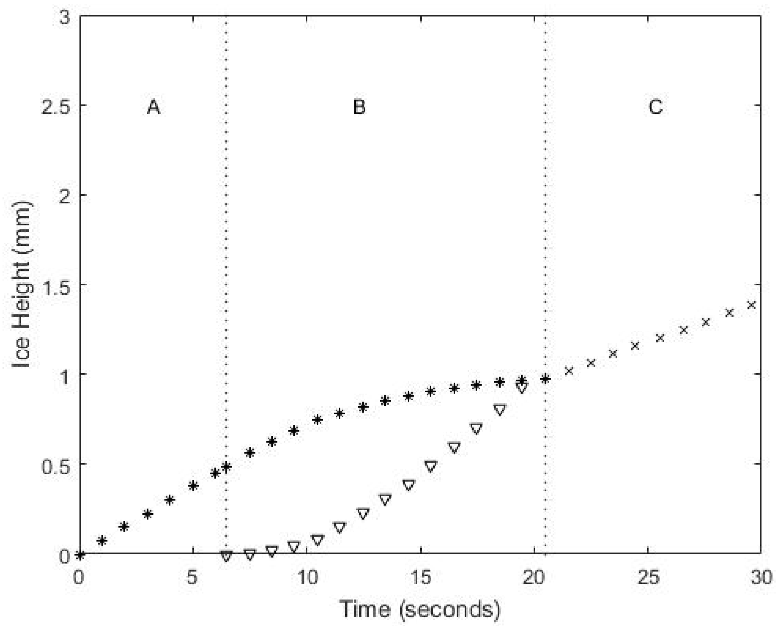

(a)

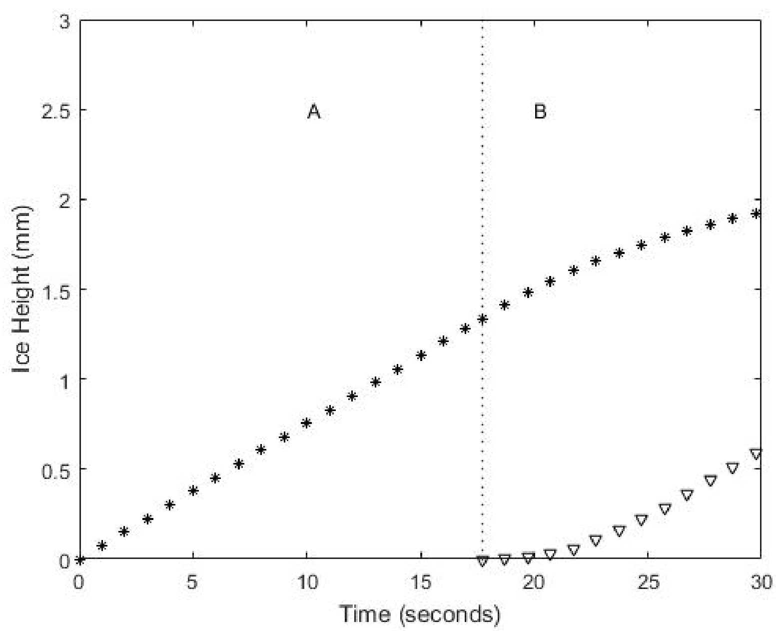

(b)

Figure 4: Mixed ice accretion at different ambient temperatures T_a and solid volume fractions ϕ respectively for 30 s of droplet impingement. The different ice and water limits are represented by the following symbols: rime ($*$), glaze ($\bigtriangledown$), mixed (x) and water film ($\circ$). (a) T_a = -3°C and $\phi = 0.65$. (b) T_a = -6°C and $\phi = 0.65$.

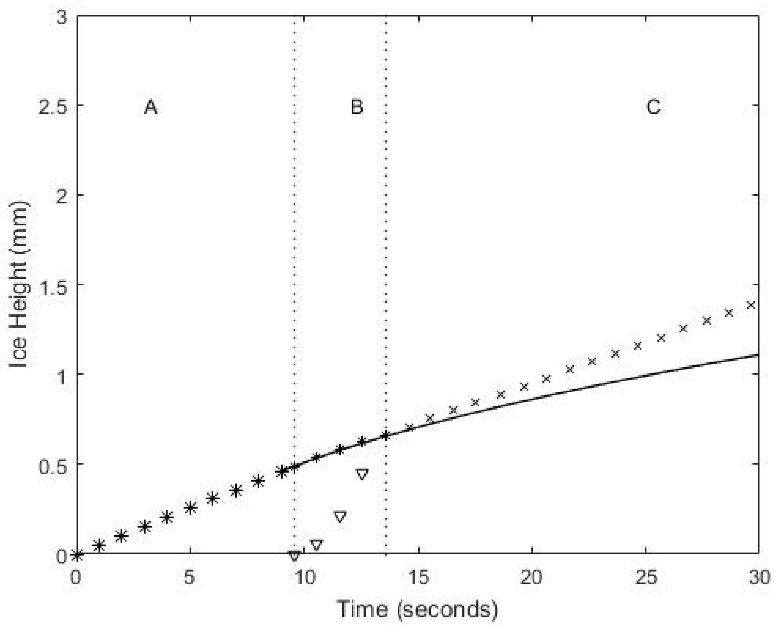

(a)

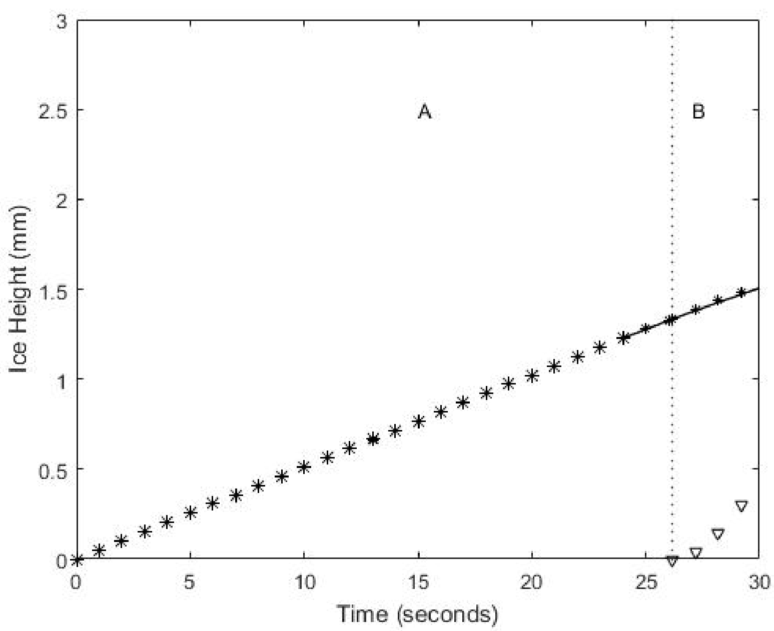

(b)

Figure 5: Mixed ice accretion model versus Myers [10] model. The different ice and water limits are represented by the following symbols: rime ($*$), glaze ($\bigtriangledown$), mixed (x) and water film ($\circ$). (a) T_a = -3°C and $\phi = 0.96$ versus Myers [10] model for glaze ice (-). (b) T_a = -6°C and $\phi = 0.96$ versus Myers [10] model for rime ($*$) and glaze ice (-).

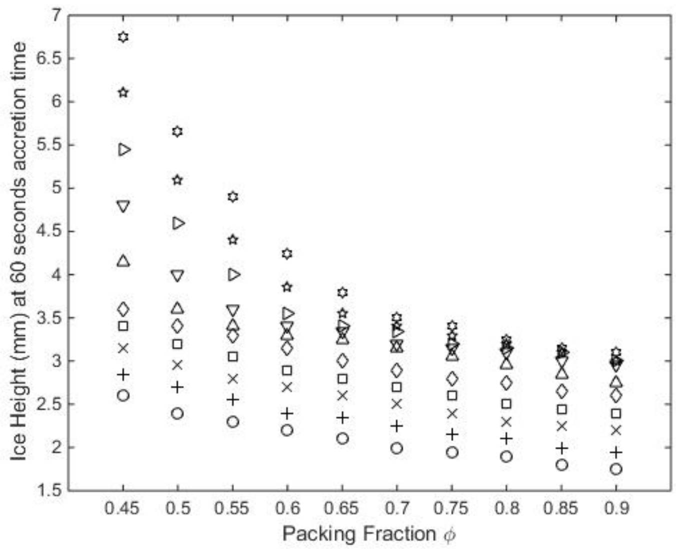

Figure 6: Overall ice height variation with changes in ϕ at -3°C (○), -6°C (◇) and -9°C (□).

temperatures. Similarly, when comparing Figure 5(a) and Figure 5(b), we can see that the decrease in temperature from -3°C to -6°C whilst the packing fraction is kept constant at 0.96 results in an overall ice height of 1.4 mm (0.7 mm glaze and 0.7 mm mixed) and 1.5 mm (0.4 mm glaze and 1.1 mm rime) respectively.

Figure 5(a) shows that although the author's model prediction results in an overall ice height of 1.4 mm as compared to the glaze model [10] height of 1.1 mm; only 0.7 mm of the former is glaze which has different adhesion characteristics than rime or mixed. Similarly Figure 5(b) shows that although the author's model prediction results in an overall ice height of 1.5 mm, exactly the same as the glaze model [10] height of 1.5 mm; only 0.4 mm of the former is glaze which has different adhesion characteristics than rime or mixed. The models match quite well even at smaller accretion times e.g. Figure 5(a) at 14 s accretion time; and limiting cases. Table 2 exhibits the differences between the author's model which consistently predicts a lower glaze ice height than the glaze ice model [10] at accretion time of 30 seconds and $\phi = 0.96$. The difference in the height of the glaze varies with ambient temperature: -2°C (33%), -3°C (30%), -4°C (31%), -5°C (7%) and -6°C (67%). The percentage fluctuations in the latter two values arise due to the completion of primary mixed ice stage at -5°C and the presence of a prolonged rime ice stage at lower temperatures of -6°C. Another key difference to note is the absence of a water film at 30 s for the author's model in all cases barring accretion at -2°C. This is because secondary mixed ice occurs due to the dual freezing actions exhibited by instantaneous freezing of a fraction of the supercooled droplets at the air-rime interface and freezing at the Stefan interface. This implies that the formation of the thin film may occur later than initially expected on an aircraft wing. In the glaze ice model [10], the water film appears immediately after the rime stage whereas in the author's model, the water film appears much later after secondary mixed ice stage.

Figure 6 exhibits the change in overall accretion height at 60 seconds with variation in ϕ. It is apparent from the figure that the height consistently increases with a reduction in ϕ. We see that the effect of packing fraction on the accretion height increases at the ambient temperature reduces.

In terms of a qualitative comparison, Myers (2001) [10] grew ice in a wind

Table 2: Ice height comparison between mixed ice accretion predicted in the present work, and a pure glaze ice accretion [10].

T_a	Glaze	Water	**Total**	Rime	Glaze	Water	Mixed	**Total**
°C	mm, *glaze only* [10]			mm, *present work*				
-2	0.9	0.6	1.5	0	0.6	0.2	0.6	1.4
-3	1	0.5	1.5	0	0.7	0	0.7	1.4
-4	1.3	0.2	1.5	0	0.9	0	0.5	1.4
-5	1.4	0.1	1.5	0	1.3	0	0.2	1.5
-6	1.5	0.1	1.6	1	0.5	0	0	1.5

tunnel in Cranfield University under conditions matching those mentioned in Table A except for a change in collection efficiency from 0.5 to 0.55. The temperature of the wind tunnel was kept at -10°C and the overall accretion time was 12 minutes. He noticed that the height of the rime ice during transition to glaze was between 2–3 mm and occurred at approximately 46 seconds. Using our predictions, a packing fraction range of 0.87–0.98 gives us an ice height of 2.9–2.6 mm at the same accretion time which is an encouraging sign covering different density values of hard rime.

It is important at this stage of the model development to also test computational results with actual experimental results in an icing facility. For this purpose, we consider two studies. Palacios et al. (2010) [29] conducted icing experiments on an Adverse Environment Rotor Test Stand (AERTS). Essentially, the experiment consisted of 1 inch diameter-50 inch radius rotor connected to a 125 HP motor; inside a cold chamber with nozzle location on the ceiling. Similar tests were conducted by Ruff (1985) [30] in the Air Force Arnold Engineering Development Center. Since solid volume fraction ϕ is

Table 3: Ice height comparison between author's model and experimental data

T_a (°C)	U_∞ $\mathrm{m\,s^{-1}}$	ρ_a $(\mathrm{g\,m^{-3}})$	t (s)	Current Model (mm)	Experimental Data (mm)	
-15	60.9	1.3	150	13.7	15.2	[30]
-13.75	60.9	1.2	300	25.3	25.4	[29]
-15	60.9	1.2	300	25.4	27.9	[30]
-12	60.9	0.8	225	12.8	13.5	[29]
-11.4	60.9	0.9	225	14.4	14	[30]
-5.5	60.9	1.3	150	4.8	5.7	[29]
-5	60.9	1.2	150	4.6	5.3	[30]

currently not linked to the freezing fraction λ in our code, we back calculate ice height from a single experimental reading of Palacios et al. (2010) [29] to give rime ice density as $743\,\mathrm{kg\,m^{-3}}$ and subsequently $\phi = 0.81$. Mean volume diameter (MVD) was fixed at 20μm and air velocity at $60.9\,\mathrm{m\,s^{-1}}$ to reduce the amount of variables during comparison with the experimental results.

AoA was kept at 0° and β was calculated from Palacios et al. (2010) [29] as $\sim$0.7. Table 3 shows the comparison of results from the author's model and experimental data. We see that for a wide array of icing conditions, discrepancies are between 0.4–15%; which is a promising sign for future work. The ice height from the experimental data was measured from the stagnation point. The errors accumulated are due to experimental calculation of collection efficiency and LWC; as well as being unable to account for changes in ϕ when LWC and ambient temperature change. This is an area of future research to build upon when λ and ϕ can be linked to compare to a wider array of experimental data.

4. Conclusion

An initial one dimensional mixed ice accretion model has been developed that incorporates both rime and glaze. A dimensionless parameter λ has been introduced to account for the accretion of mixed ice on an aerofoil in nature. Current icing models account for individual rime and glaze ice accretion on an aircraft wing. The development of a mixed ice model is the first step in quantifying the accretion of the third type of in-flight icing seen in nature and shows that for similar atmospheric parameter ranges, this simple mixed ice description leads to very different accretion rates. The boundary temperatures provided for the atmosphere in relation to the type of icing experienced correspond well with the literature. The authors' mixed ice model reduces to the glaze ice model [10] when $\lambda = 0$ and states that the model [10] is valid only for temperatures between -1.8° and 0°C. It predicts lower glaze ice heights than the former at lower temperatures. Lower temperatures favour higher ice growth and increasing the packing fraction corresponds to lower ice height and glaze icing regime. The model shows a promising comparison with both previously published computational data and experimental results.

Future work will include determining a transient value of freezing fraction to provide results for longer accretion times, changing water film temperatures and the effect of droplet size. The freezing fraction must also be linked to the packing fraction to allow for variation in ϕ. Eventually, the model must be expanded to account for two-dimensional accretion on an aircraft wing.

Acknowledgements

This study was conduced as a part of EU Clean Sky program ICECOAT (JTI-CS-2012-2-SFWA-01-051).

Table A: Notation and values ascribed to parameters throughout this paper [20].

Parameter	Value
a	0.895
c_a	$1014\,\mathrm{J\,kg^{-1}K^{-1}}$
H_{aw}	$500\,\mathrm{W\,m^{-2}K^{-1}}$
L_f	$334000\,\mathrm{J\,kg^{-1}}$
c_w	$4220\,\mathrm{J\,kg^{-1}K^{-1}}$
x_e	$9.53\,\mathrm{m\,s^{-1}}$
e_0	$44.4\,\mathrm{Pa\,K^{-1}}$
ρ_l	$0.001\,\mathrm{kg\,m^{-3}}$
β	0.5
U_∞	$90\ \mathrm{m\,s^{-1}}$
α	$0°$
ρ_w	$1000\,\mathrm{kg\,m^{-3}}$
ρ_i	$917\,\mathrm{kg\,m^{-3}}$
T_f	$273.15\,\mathrm{K}$
k_i	$2.18\,\mathrm{W\,m^{-1}K^{-1}}$
k_w	$0.571\,\mathrm{W\,m^{-1}K^{-1}}$
$\dot{M}$	$0.045\,\mathrm{kg\,m^{-2}s^{-1}}$
x_s	$11.65\,\mathrm{m\,s^{-1}}$

Appendix

4.1. Mass Flux of Droplets

Fig. 1(a) exhibits the supercooled droplet mass flux prior to the accretion stage. The first step for the icing code is to define the different terms in the mass balance. The rate of impinging droplets incident on an aircraft wing $\dot{N}$ can be expressed as

$$\dot{N} = \frac{V_{air}\rho_l\beta}{V_d\rho_w}, \tag{36}$$

where $V_d = \frac{\pi d^3}{6}$ is the volume of a single (spherical) droplet and V_{air} is the volume of air incident on the aircraft wing per second. β i.e. the collection efficiency, can be defined as the distance between two droplets in the free stream and along the body surface when they impact the aerofoil respectively [12]. V_{air} is given by,

$$V_{air} = AU_\infty \cos\alpha, \tag{37}$$

where α is the angle of attack. Beyond $\alpha = 20°$, the aircraft begins to stall. Hence α generally ranges between 5° and 15°. The incoming mass flux of supercooled droplets incident per unit area of the wing $\dot{M}$ can be defined as

$$\dot{M} = \frac{V_d \dot{N} \rho_w}{A}, \tag{38}$$

which reduces to

$$\dot{M} = \beta U_\infty \rho_l \cos(\alpha). \tag{39}$$

For one-dimensional accretion on a flat plate, $\alpha = 0$. Using the values from Table A, we get $\dot{M} = 0.045\,\mathrm{kg\,m^{-2}s^{-1}}$.

References

[1] Messinger B.L. Equilibrium temperature of an unheated icing surface as a function of air speed. *Journal of Aeronautical Sciences*, pages 29–42, 1953.

[2] Poots G.I. Ice and snow accretion on structures. *Research Studies Press*, 1996.

[3] Bourgault Y., Beaugendre H., and Habashi W.G. Development of a shallow-water icing model in fensap-ice. *Journal of Aircraft*, 37(4):640–646, 2000.

[4] Brakel T.W., Charpin J.P.F., and Myers T.G. One-dimensional ice growth due to incoming supercooled droplets impacting on a thin conducting substrate. *International Journal of Heat and Mass Transfer*, 50:1694–1705, 2007.

[5] Cao Y., Ma C., Zhang Q., and Sheridan J. Numerical simulation of ice accretions on an aircraft wing. *Aerospace Science and Technology*, 23:296–304, 2012.

[6] Rios M. Icing simulations using Jones' density formula for accreted ice and lewice. *29th Aerospace Sciences Meeting*, Reno, Nevada, U.S.A., 1991.

[7] Myers T., Thompson C., and Bandakhavai V.K.S.S. Modelling water flow on aircraft in icing conditions Part 1: Theory and results. In *15th IMACS World Congress on Scientific Computation Modelling and Applied Mathematics*, Germany, 1997. Wissenschaft and Technik.

[8] Myers T.G. and Thompson P. Modelling the flow of water on aircraft in

icing conditions. *American Institute of Aeronautics and Astronautics*, 36(6):1010–1013, 1998.

[9] Myers T.G. and Hammond D.W. Ice and water film growth from incoming supercooled droplets. *International Journal of Heat and Mass Transfer*, 42:2233–2242, 1999.

[10] Myers T.G. Extension to the messinger model for aircraft icing. *AIAA Journal*, 39(2):211–218, 2001.

[11] Myers T.G., Charpin J.P.F., and Thompson C.P. Slowly accreting ice due to supercooled water impacting on a cold surface. *Physics of Fluids*, 14(1):240–256, 2002.

[12] Verdin P. *An Automatic Multi-Stepping Approach for Aircraft Ice Prediction*. PhD thesis, Cranfield University, 2007.

[13] Stefan J. ber die theorie der eisbildung insbesondere ber die eisbildung im polarmeere sitzungsberichte der kaiserlichen akademie der wissenschaften mathematische-naturwissenschaftliche. *Classe II Abtheilung*, 98:965–983, 1889.

[14] Zhang X., Wu X., and Min J. Aircraft icing model considering both rime ice property variability and runback water effect. *International Journal of Heat and Mass Transfer*, 104:510–516, 2017.

[15] Xin L., Junqiang B., Jun H., Kun W., and Yang Z. A spongy icing

model for aircraft icing. *Chinese Journal of Aeronautics*, 27(1):40–51, 2014.

[16] Worster M.G. Convection in mushy layers. *Annual Review of Fluid Mechanics*, 29:91–122, 1997.

[17] Anderson D.N. and Feo A. Ice-accretion scaling using water-film thickness parameters. *American Institute of Aeronautics and Astronautics*, 40th AIAA Aerospace Sciences Meeting and Exhibit,(Reno, Nevada, U.S.A.), 2002.

[18] Williams E.R. and Zhang R. Density of rime in laboratory simulations of thunderstorm microphysics and electrification. *Journal of Geophysical Research*, 101(D23):29715–29719, 1996.

[19] Ya Yi Dong and John Hallett. Droplet accretion during rime growth and the formation of secondary ice crystals. *Quarterly Journal of the Royal Meteorological Society*, 115(485):127–142, 1989.

[20] Myers T.G. and Charpin J.P.F. A mathematical model for atmospheric ice accretion and water flow on a cold surface. *International Journal of Heat and Mass Transfer*, 47:5483–5500, 2004.

[21] Battisti L. *Wind Turbines in Cold Climates - Icing Impacts and Mitigation Systems*. Springer International Publishing, New Delhi, India, 2015.

[22] Lynch F. T. and Khodadoust A. Effect of ice accretions on aircraft aerodynamics. *Progress in Aerospace Sciences*, 37:669–767, 2001.

[23] Mirzaei M., Ardekani M. A., and Doosttalab M. Numerical and experimental study of flow field characteristics of an iced aerofoil. *Aerospace Science and Technology*, 13:267–276, 2009.

[24] Politovich M.K. Aircraft icing. *Encyclopaedia of Atmospheric Sciences*, pages 68–75, 2003.

[25] Worster M.G. *Perspectives in Fluid Dynamics: A Collective Introduction to Current Research (edited by. G.K. Batchelor, H.K. Moffatt and M.G. Worster)*, chapter Solidification of fluids, pages 393–446. Cambridge University Press, 2000.

[26] Valarezo W.O. Aerodynamic performance effects due to small leading edge ice (roughness) on wings and tails. *Journal of Aircraft*, 30(6):807–812, 1993.

[27] Binzaid S., Al-Tomal S.A., Zaid D., and Rosen M.H. Deicing technology for modern military and commercial aircraft wing surfaces. In *Electrical and Electronic Engineering Proceedings of the Conference on Engineering Research, Innovation and Education 2011*, Sylhet, Bangladesh, 11-13 January 2011. CERIE.

[28] Gao H. and Rose J.L. Ice detection and classification on an aircraft wing

with ultrasonic shear horizontal guided waves. *IEEE Transactions on Ultrasonics, Ferroelectrics and Frequency Control*, 56(2):334–344, 2009.

[29] Palacios J.L., Brouwers E.W., Han Y., and Smith E.C. Adverse environment rotor test stand calibration procedures and ice shape correlation. *American Helicopter Society 66th Annual Forum, Phoenix, AZ, May 11-13*, 2010.

[30] Ruff G. Analysis and verification of the icing scaling equations. *Air Force Technical Report AEDC-TR-85-30*, November 1985.